Global NEST Journal, **28** (XX), pp 1-15
Available online: 16/06/2026

Analysis of Extreme Rainfall based on Atmospheric Dynamics of Tropical Cyclone SENYAR using WRF-ARW

Sorja Koesuma[1,2]*, Richard Mahendra Putra[3], Delfina Azzahra Kusuma[4], Angger Zufan Hanggara[1] and Rahmat Gernowo[5]

[1]Department of Physics, Sebelas Maret University, Surakarta, Indonesia
[2]Disaster Research Centre, Sebelas Maret University, Surakarta, Indonesia
[3]Meteorology, Climatology, and Geophysical Agency, Jakarta, Indonesia
[4]Department of Ocean Engineering, Bandung Institute of Technology, Bandung, Indonesia
[5]Department of Physics, Diponegoro University, Semarang, Indonesia

*Correspondence e-mail: sorja@staff.uns.ac.id

Abstract

Tropical Cyclone SENYAR represents a rare landfalling event in the Indonesian region, where tropical cyclones seldom reach land. This study aims to (1) simulate the lifecycle evolution of SENYAR using the WRF-ARW model at 27/9 km resolution, (2) quantify model accuracy against IBTrACS best-track data, and (3) identify the dynamical drivers of extreme rainfall over northern Sumatra. The pre-genesis phase was characterized by warm sea surface temperatures (>28.5°C), increasing CAPE (>2000 J kg^{-1}), relative vorticity (>10×10^{-5} s^{-1}), and weak vertical wind shear (<10 m s^{-1}). The mature phase exhibited a well-organized cyclonic structure with closed isobars, deep moisture columns, and intense winds around the eye, while landfall triggered rapid decay through moisture depletion and increased shear sensitivity. Quantitative evaluation against IBTrACS revealed systematic biases: the WRF model underestimated minimum sea level pressure by a mean bias of −11.38 hPa (MAE = 11.38 hPa, RMSE = 13.65 hPa) and overestimated maximum wind speed by +28.08 kt (MAE = 28.08 kt, RMSE = 31.92 kt). Spatially averaged winds within a 100-km radius showed better agreement, indicating that the overestimation is concentrated near the cyclone core. Extreme rainfall exceeding 200 mm/day over Aceh and North Sumatra coincided with maximum moisture convergence during the mature-to-landfall transition, not with peak wind intensity. Despite intensity biases, WRF successfully captured the mesoscale dynamics governing SENYAR's lifecycle and associated hydrometeorological impacts. These findings provide quantitative benchmarks for WRF calibration in equatorial environments and underscore the need for multi-physics ensemble and hydrological coupling to improve early warning for rare but high-impact cyclones in Indonesia.

Keywords: Tropical Cyclone, WRF, Landfall, Extreme Rainfall.

Received: 21/01/2026,

Accepted: 31/05/2026,

Available online: 16/06/2026

Graphical abstract

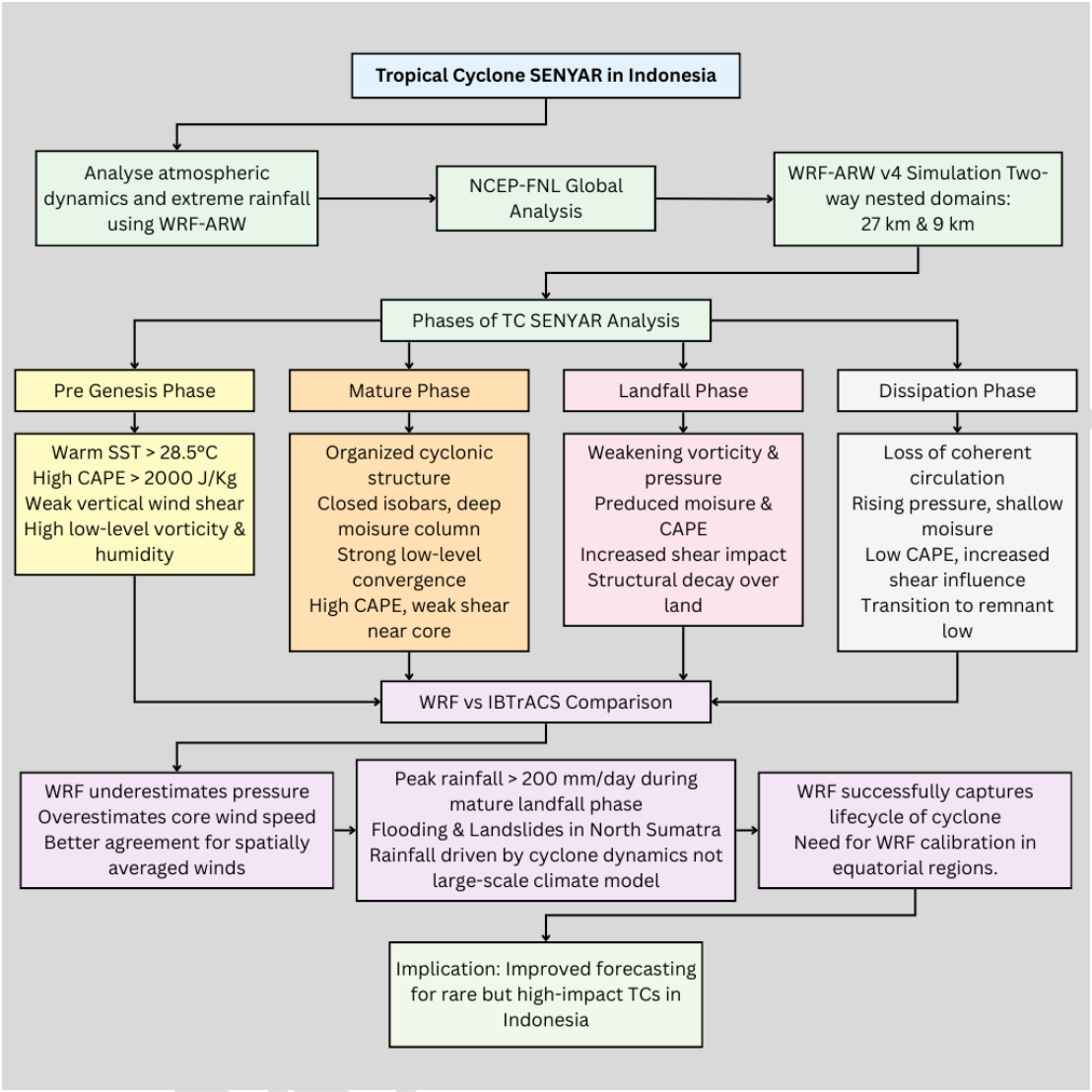

1. Introduction

Tropical cyclones (TCs) are among the most destructive atmospheric phenomena, posing severe threats to coastal populations and infrastructure. Although the global frequency of TCs has remained relatively stable, the proportion of storms reaching higher intensity levels has increased significantly under ongoing climate change (Singh *et al.*, 2025). Socio-economic impacts are substantial, particularly in densely populated regions such as the Pearl River Delta (Li *et al.*, 2024) and Bangladesh (Rahman *et al.*, 2024).

Although tropical cyclones are rare in Indonesia, recent studies indicate that their impact in the region is increasing. Events such as Cempaka (2017) and the more devastating Seroja (2021) demonstrate this heightened vulnerability (Krisnayanti *et al.*, 2022; Sekaranom & Putri, 2021). Multi-decade analyses have also revealed a southward shift in cyclone activity (Tridaiana & Marzuki, 2023), thereby increasing risks to Indonesian territories. However, the dynamics and extreme rainfall impacts of cyclones making landfall in Indonesia remain poorly understood, particularly regarding high-resolution modeling approaches with explicit evaluation of physics scheme performance.

Forecasting the structure and intensity of tropical cyclones (TCs) is still very difficult because of the complicated internal dynamics and interactions between the ocean and the atmosphere (Lee *et al.*, 2024; Bousquet *et al.*, 2021). Recent advances in data-driven and AI-based models have shown promise for long-term rainfall prediction (Prasad *et al.*, 2024; Subramanian *et al.*, 2024) and flood forecasting using meteorological variables and remote sensing imagery (Kumar & Singh, 2024; Sharma *et al.*, 2025; Al-Biruni, 2025; Venkatraman *et al.*, 2024). However, their application to TC-induced extreme rainfall in equatorial regions remains unexplored. High-resolution numerical models, such as the Weather Research and Forecasting (WRF) model, are essential for addressing this challenge because they can capture mesoscale and convective processes within the cyclone core. Previous studies have demonstrated that finer WRF-ARW resolution significantly reduces track and

intensity errors (Osuri *et al.*, 2013). However, knowledge gaps remain, particularly regarding cyclones of moderate intensity or quasi-stationary tracks near the coast. Global models often fail to resolve fine-scale processes in these situations, such as eyewall formation and sharp pressure gradients. Predicting rapid intensification remains a major challenge as well (Singh *et al.*, 2025).

While previous studies have examined tropical cyclone structure and intensity in Indonesian regions (e.g., Cempaka 2017, Seroja 2021), the specific case of Tropical Cyclone SENYAR—a rare equatorial landfalling cyclone in the Malacca Strait—has not been analyzed using high-resolution WRF-ARW simulations. To our knowledge, no prior WRF-based study has systematically examined the lifecycle dynamics of a cyclone making landfall in the Malacca Strait region. The novelty of this study lies in three key aspects: (1) a phase-specific analysis of SENYAR's lifecycle (pre-genesis, mature, landfall, dissipation) using an integrated set of dynamical and thermodynamical variables (CAPE, relative vorticity, vertical wind shear, relative humidity, sea surface temperature, and wind fields); (2) systematic evaluation of a specific physics parameterization suite (Purdue-Lin microphysics, Kain-Fritsch cumulus, YSU boundary layer) against IBTrACS best-track data, which identified systematic biases in minimum sea level pressure and maximum wind speed; and (3) explicit linkage of phase-dependent cyclone dynamics to observed extreme rainfall patterns (>200 mm/day) over northern Sumatra, demonstrating that moisture convergence during the mature-to-landfall transition, rather than wind intensity alone, governs hydrometeorological impacts in equatorial regions. By systematically analyzing each phase of SENYAR's evolution with these specific variables and chosen schemes, this work establishes a physically coherent framework linking cyclone dynamics, moisture convergence, and rainfall extremes.

Quantitatively, this study aims to (1) quantify the bias in WRF-simulated minimum sea level pressure (MSLP) and maximum wind speed (Vmax) relative to IBTrACS, (2) determine the threshold of convective available potential energy (CAPE >2000 J kg^{-1}) and relative vorticity (>10×10^{-5} s^{-1}) associated with cyclogenesis, and (3) evaluate the model's ability to reproduce extreme rainfall rates exceeding 200 mm/day over northern Sumatra, with future research needed to calibrate these WRF schemes for equatorial operational use and to integrate rainfall forecasts into impact-based early warning systems—a contribution that extends beyond previous descriptive studies of tropical cyclones in Indonesia.

2. Data And Methods

2.1. *Observational Data*

This study employed the NCEP Final (FNL) Operational Global Analysis dataset, which provides global atmospheric analyses on a 1° × 1° grid at 6-hourly intervals. The dataset is generated by the Global Data Assimilation System (GDAS), which continuously assimilates observations from the Global Telecommunications System (GTS) and other in situ and remote-sensing sources to produce high-quality global fields. These FNL analyses include key meteorological variables such as sea-level pressure, temperature, humidity, and wind components across multiple pressure levels. The data were used both as the initial and lateral boundary conditions for the numerical simulation of Tropical Cyclone SENYAR.

2.2. *WRF-ARW model*

This study used the Weather Research and Forecasting (WRF-ARW) model version 4 (Skamarock *et al.*, 2019) to dynamically downscale NCEP-FNL data in order to capture mesoscale cyclone features. The WRF-ARW framework has been extensively applied for diverse meteorological studies, including the simulation of extreme rainfall events (Biswasharma *et al.*, 2024), severe convective storms (Spiridonov *et al.*, 2020), and regional wind field variations (Nguyen *et al.*, 2023). The model can also be coupled with chemical and aerosol modules (WRF-Chem) to simulate air pollutant concentrations (Silva *et al.*, 2026).

The experimental design consisted of a continuous simulation run initialized at 00:00 UTC on 23 November 2025 and integrated over a period of 156 hours. The modeling framework utilized a two-way nested domain configuration. The outer domain (d01), designed to capture large-scale synoptic forcing, was configured with a horizontal grid spacing of 27 km and dimensions of 99 × 99 grid points. The inner domain (d02), centered over the cyclone genesis region to explicitly resolve mesoscale internal dynamics, utilized a refined resolution of 9 km with 177 × 177 grid points. Both domains employed 34 vertical levels from the surface up to a model top of 50 hPa.

Table 1. Physical Parameterization of WRF model.

Physical parameterization scheme	Outer domain	Inner Domain
Microphysics	Purdue–Lin Scheme	Purdue–Lin Scheme
Longwave Radiation	RRTM Scheme	RRTM Scheme
Shortwave Radiation	Dudhia Scheme	Dudhia Scheme
Planetary Boundary Layer	Yonsei University Scheme	Yonsei University Scheme
Cumulus	Kain - Fritsch Scheme	Kain - Fritsch Scheme

2.3. *Physical Parameterization Schemes*

A consistent set of physical parameterization schemes was applied across both domains to ensure dynamical coherence between scales. Microphysical processes were represented using the Purdue–Lin microphysics scheme (Chen & Sun, 2002). Longwave radiative transfer was simulated using the Rapid Radiative Transfer Model (RRTM) (Mlawer *et al.*, 1997), while shortwave radiation

was parameterized using the Dudhia scheme (Dudhia, 1989). Turbulent mixing within the planetary boundary layer was treated using the Yonsei University (YSU) scheme (Hong *et al.*, 2006), and subgrid-scale convective processes were parameterized using the Kain–Fritsch scheme (Kain, 2004). All physical schemes were applied consistently in both the coarse-and high-resolution domains (Ikram *et al.*, 2022).

2.4. *Evaluation Metrics*

For quantitative evaluation, we compare WRF-simulated MSLP and Vmax against IBTrACS best-track data using three metrics: bias (simulated minus observed), mean absolute error (MAE), and root mean square error (RMSE). These are defined as follows:

$$MBE = \left(\frac{1}{n}\right)\Sigma\left(S_i - O_i\right)$$

$$MBE = \left(\frac{1}{n}\right)\Sigma\left(S_i - O_i\right)$$

$$RMSE = \sqrt{\left(\frac{1}{n}\right)\Sigma\left(S_i - O_i\right)^2}$$

where S_i is the simulated value (either minimum sea level pressure or maximum wind speed) at time step i, O_i is the corresponding observed value from IBTrACS, and **n** is the total number of matching time steps over the cyclone's lifecycle (pre-genesis, mature, landfall, and dissipation phases). Positive MBE indicates overestimation by the model, while negative MBE indicates underestimation. MAE and RMSE quantify the average magnitude of error, with RMSE giving greater weight to larger deviations. Extreme rainfall is defined as daily precipitation exceeding 200 mm, based on BMKG's threshold for heavy-to-extreme rainfall warnings. Additionally, we compute the spatial correlation between WRF-simulated rainfall fields and rain gauge observations from three stations (Malikussaleh, Maimun Saleh, Iskandar Muda) to quantify model performance in reproducing observed extremes.

3. Result And Discussion

3.1. *Comparison of WRF Output and IBTrACS Data*

A comparison of intensities between WRF simulations and IBTrACS best-track data reveals consistent biases. Specifically, the WRF model tends to simulate lower minimum sea-level pressures and higher maximum wind speeds than observed, particularly during the mature and early landfall phases (**Figures 1 and 2**). These include Mean Bias Error (MBE), Mean Absolute Error (MAE), andRoot Mean Square Error (RMSE) are summarized in **Table 2**.

Table 2. Statistical metrics of WRF-ARW simulations

Variable	MBE	MAE	RMSE
Minimum Sea-Level Pressure (hPa)	-11.38	11.38	13.65
Maximum Wind Speed (kt)	28.08	28.08	31.92

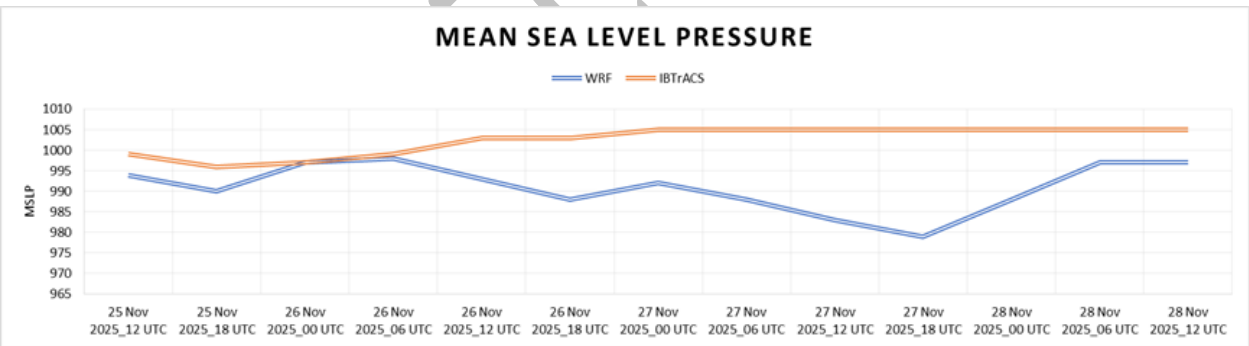

Figure 1. Comparison of MSLP during Tropical Cyclone SENYAR

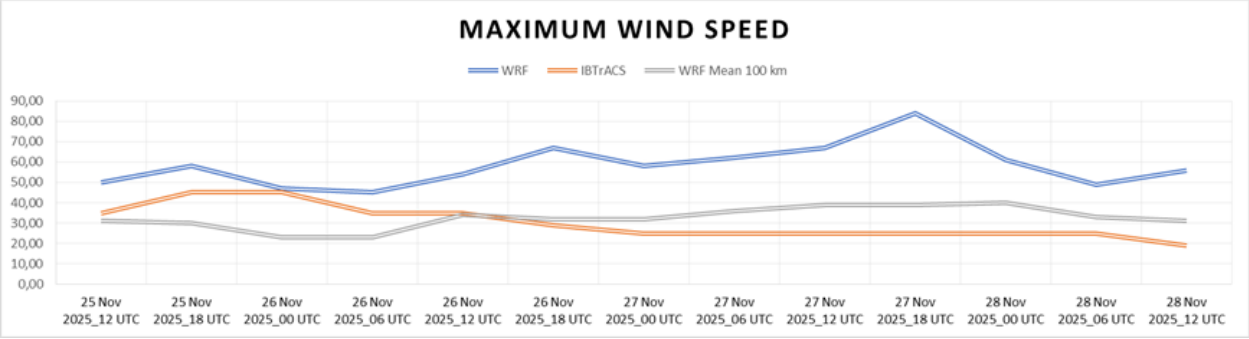

Figure 2. Comparison of wind speed during Tropical Cyclone SENYAR

The metrics confirm systematic biases in the WRF simulation. The model underestimated minimum sea-level pressure by an average of 11.38 hPa and overestimated maximum sustained wind speed by 28.08 kt. These biases are most pronounced during the mature phase and immediately after landfall, when the model produces stronger pressure gradients and more intense low-level winds around the cyclone core.

However, this bias is scale-specific. When winds are averaged within a 100-km radius of the cyclone center, there is significantly better agreement between WRF and IBTrACS. This suggests that the overestimation of wind speeds is primarily concentrated within the cyclone's core, where WRF can resolve convective structures and extreme pressure gradients, which are smoothed out in the observational dataset.

These differences reflect the model's sensitivity to the choice of physical parameterization schemes, as well as WRF's capability to represent mesoscale processes at high resolution. Three potential causes are considered. First, the specific combination of Purdue-Lin microphysics, Kain-Fritsch cumulus, and YSU boundary layer may overestimate diabatic heating and surface enthalpy fluxes, leading to stronger simulated vorticity (Shenoy *et al.*, 2021). Second, the 9-km inner domain resolution, while adequate for mesoscale structure, cannot fully resolve the sharp eyewall pressure gradient; sensitivity studies show that finer grids (≤3 km) significantly reduce intensity bias. Third, IBTrACS data itself carries uncertainties (5–10 kt) due to heterogeneous observation platforms and estimation methods, especially in data-sparse regions like the Malacca Strait. Despite these biases, WRF qualitatively captures SENYAR's lifecycle, making it a valid tool for process studies, though future sensitivity analyses with alternative physics schemes and higher resolution are recommended.

3.2. *Lifecycle Evalution of TC Senyar*

The results are presented by following the temporal evolution of Tropical Cyclone SENYAR, from the pre-genesis disturbance stage through maturity, landfall, and eventual dissipation. For each phase, key dynamical and thermodynamical parameters derived from WRF simulations are examined to elucidate the mechanisms controlling cyclone development. Importantly, these parameters are interpreted in the context of their role in modulating moisture convergence, convective intensity, and rainfall distribution, thereby providing a coherent framework for understanding how the evolving cyclone dynamics contribute to extreme rainfall over northern Sumatra.

3.2.1. Disturbance Phase

WRF analysis shows that pre-genesis maritime environment of SENYAR was dominated by favorable thermodynamic conditions, particularly sea surface temperatures (SST) that consistently exceeded 28.5°C in the Malacca Strait (**Figure 3**). These warm conditions provided the main foundation for the development of the subsequent system.

At 00 UTC on November 24, 2025, SST values of approximately 28.5°C exceeded the generally accepted threshold for tropical cyclone formation. This indicates that ocean heat availability was a dynamic factor supporting the growth stage of tropical cyclone SENYAR. The spatial continuity of consistently warm SSTs for 2 days indicates that the developing system remained within a broad body of warm water, allowing for sustained surface fluxes to support convective activity as atmospheric conditions gradually became more favorable.

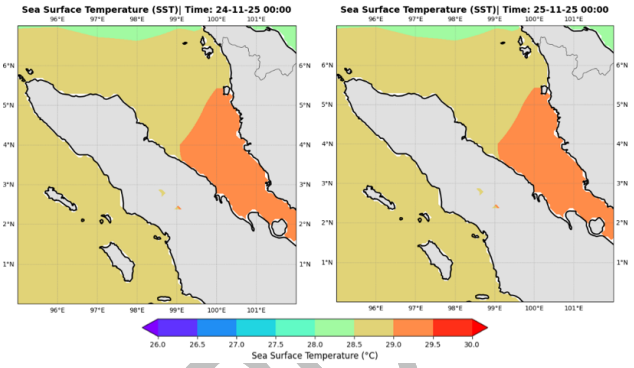

Figure 3. Sea surface temperature (SST) over the Malacca Strait on 24–25 November 2025 during the pre-genesis phase.

Analysis of the climatic conditions during the lifecycle of Tropical Cyclone SENYAR (November 2025) reveals that the observed extreme rainfall was driven primarily by the storm's internal dynamics rather than by large-scale climate variability. While the Asian Winter Monsoon and Madden-Julian Oscillation (MJO) likely provided a background of enhanced moisture across the Maritime Continent, these broad-scale factors alone cannot account for the localized intensity (Permana, 2021; Fauzi & Hidayat, 2018). According to the Indonesian Agency for Meteorology, Climatology, and Geophysics (BMKG), the El Niño-Southern Oscillation (ENSO) index was recorded at -0.80, signifying a weak La Niña condition, while the Indian Ocean Dipole (IOD) remained in a neutral-to-negative phase with a value of -0.36. These indices imply that the observed extreme rainfall anomalies were not driven primarily by global circulation forcing or long-range moisture transport from the Indian Ocean (Hanifa & Wiratmo, 2024). Instead, WRF-ARW simulations corroborate that the precipitation intensity was predominantly attributed to the cyclone's mesoscale convective system, internal vorticity, and intense air-sea fluxes. These mechanisms concentrated moisture convergence far beyond the baseline levels typically associated with MJO or monsoonal influence (Rusli, 2026; Camargo *et al.*, 2020).

These warm ocean conditions are accompanied by increased atmospheric instability, as reflected in the evolution of the Convective Available Potential Energy (CAPE). At 00 UTC on November 24, 2025 shown at **Figure 4**, the CAPE value over the Strait of Malacca exceeded 1000 J kg^{-1}, indicating a sufficiently unstable atmosphere capable of supporting deep convection. Although convection at this stage of highly convective conditions is still widespread, the presence of a high CAPE highlights the increasing thermodynamic potential for convection development. At 00 UTC on November 25, 2025, the CAPE value increased significantly to above 2000 J kg^{-1}, indicating a significant

increase in convective instability across the ocean region between Sumatra and Peninsular Malaysia. This increase provides a more favorable environment for sustained, deeper convective updrafts, potentially leading to the formation of tropical cyclones.

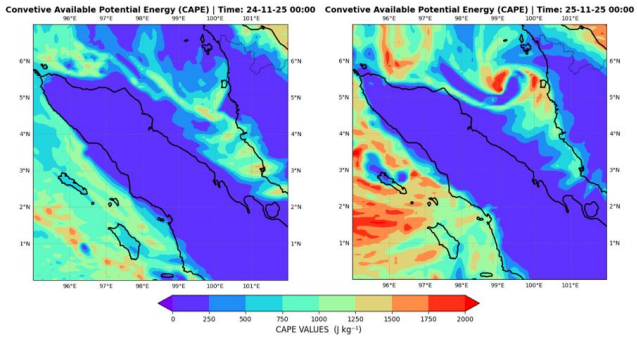

Figure 4. CAPE (J kg^{-1}) on 24–25 November 2025 showing increasing convective instability prior to cyclogenesis.

During the disturbance phase, 850-hPa relative vorticity values **(Figure 5)** were mostly positive and exceeded 10 x 10^{-5} s^{-1}, indicating a favorable dynamic environment for cyclogenesis. At 00 UTC 24 November, this elevated vorticity lacked a corresponding surface pressure minimum, due to the unfavorable sea level pressure conditions, indicated by the absence of closed isobars. This suggests that on November 24, 2025, despite the development of rotational motion, the system had not yet achieved sufficient convective organization and diabatic heating to generate a consolidated surface response.

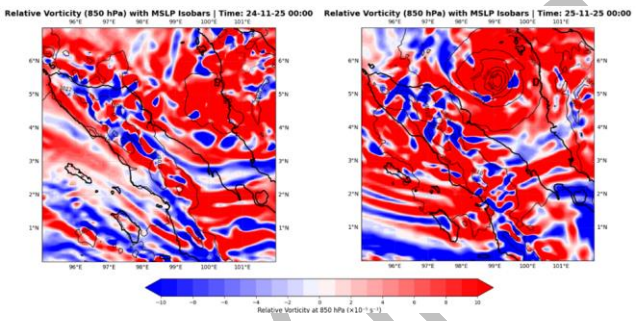

Figure 5. Relative vorticity at 850 hPa and mean sea level pressure on 24-25 November 2025.

Meanwhile, at 00 UTC on 25 November 2025, a clearer dynamical linkage emerged. The region of high relative vorticity became closer to the lower surface pressure over the Strait of Malacca, reflecting intense low-level convergence and more effective mass redistribution. Furthermore, the sea level pressure also decreased significantly, forming closed isobars, indicating the presence of a fairly intense convective system in the area. This condition also marked a crucial transition to cyclogenesis, as the developing vortex began to exhibit characteristics of a dynamically coherent system.

Moisture availability further enhances this transition. Relative humidity values **(Figure 6)** in the lower to middle troposphere exceeded 80% during both analysis periods, providing a humid environment conducive to sustained convection. When analyzed in conjunction with lower-layer wind patterns, relative humidity and wind patterns provide insight into whether moisture-rich air is dynamically organizing and converging toward the disturbance center. At 850 hPa, wind circulation patterns reveal the extent of lower-layer convergence and cyclonic rotation, both of which are crucial for the initiation and maintenance of organized convection during the pre-genesis stage.

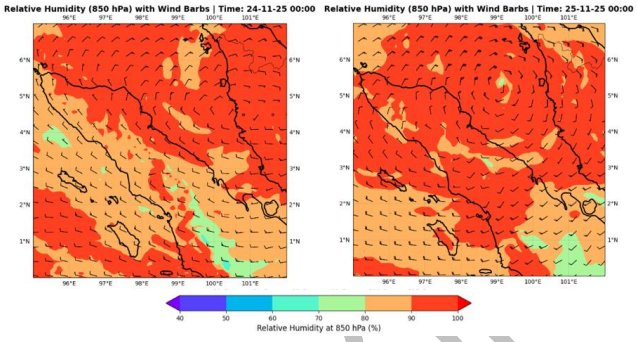

Figure 6. Relative humidity at 850 hPa and wind vectors on 24-25 November 2025.

Based on WRF simulations at 00 UTC on 24 November 2025, the 850-hPa wind field indicates that the disturbance is still characterized by weak and poorly organized flow, with no clear cyclonic circulation. Although relative vorticity is already positive at this stage, the wind vectors have not yet shown any rotation, indicating a strengthening of the developing cyclonic system. Nevertheless, the relative humidity distribution shows values exceeding 80% over a large area around the disturbance. This humid environment is favorable for convective development; however, the lack of organized low-level convergence indicates that convective activity remains sporadic and not sufficiently linked to the underlying dynamical structure. Furthermore, at 00 UTC on November 25, 2025, a significant change in the low-level wind structure is evident in the WRF results. The 850-hPa wind vectors exhibit a clear counterclockwise rotation over the Strait of Malacca region, indicating the formation of a cyclonic circulation consistent with Northern Hemisphere dynamics. This organized wind pattern reflects increased low-level convergence and the strengthening of the initial vortex. Concurrently, relative humidity remains high, with values exceeding 80% around the circulation center. The high moisture availability and well-defined cyclonic wind structure indicate that deep convection continues to develop and dynamically generates low-level circulation.

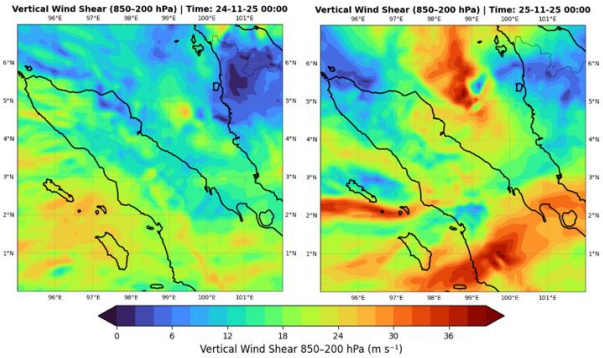

Figure 7. Vertical wind shear (200–850 hPa, m s^{-1}) on 24-25 November 2025.

The evolution of vertical wind shear **(Figure 7)** further modulates these processes. At 00 UTC on 24 November

2025, vertical wind shear between 200 and 850 hPa remains relatively weak, providing a favorable environment for the vertical alignment of convection and low-level circulation. Although shear values increase in the surrounding region by 00 UTC on 25 November 2025, a localized shear minimum persists near the developing system core. This low-shear environment is crucial in maintaining vertical coherence, enabling organized convection to efficiently reinforce the low-level circulation despite less favorable large-scale conditions.

During the pre-genesis phase of Tropical Cyclone SENYAR, the WRF-simulated wind field indicated the early development of a cyclonic circulation, characterized by weak counterclockwise flow consistent with Northern Hemisphere dynamics. Although this pattern indicated the beginning of such a disturbance, wind speeds remained relatively low and had not yet reached the values characteristic of a fully developed tropical cyclone.

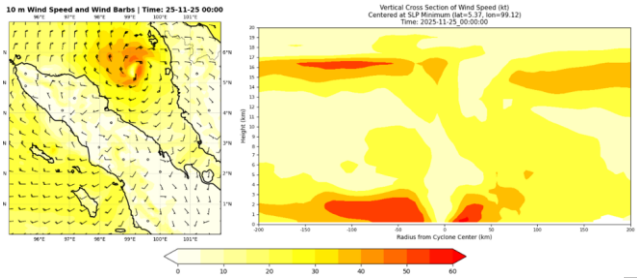

Figure 8. Horizontal wind speed and streamlines at 850 hPa on 25 November 2025, 00 UTC.

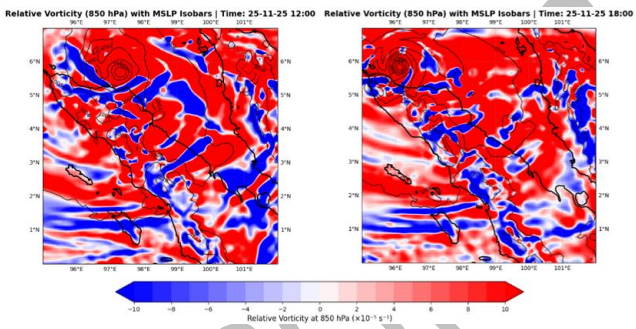

Figure 9. Relative Vorticity with Mean Sea Level Pressure on 25 Nov 2025 at 12 and 18 UTC.

Spatial wind cross sections **(Figure 8)** revealed that the region of increased wind speeds was confined to a small area near the newly formed center, while vertical cross sections indicated that stronger winds were confined to shallow layers in the lower troposphere. The limited horizontal and vertical extent of these maximum winds indicated weak circulation conditions and the presence of convection currents, but not yet particularly strong, confirming that the system remained dynamically immature despite the emergence of cyclonic flow.

In summary, the pre-genesis evolution of Tropical Cyclone SENYAR was characterized by persistently warm sea surface temperatures (SSTs) that formed a strong thermodynamic basis, followed by increasing convective instability, increasing moisture availability, strengthening of bottom-layer vorticity, and locally favorable vertical wind shear. In addition to these factors, the near-surface and lower-troposphere wind fields had shown the emergence of a cyclonic circulation pattern, indicating that cyclone development was progressing. However, wind speeds during this stage were still weak and cyclonic flow was spatially restricted, reflecting an immature system characterized by limited horizontal and vertical winds. Dynamic conditions at the time with wind structure had begun to develop, but had not yet fully organized as a tropical cyclone. Then on November 25, 2025, a transition occurred from a weak disturbance to a more dynamically organized system with a high potential for tropical cyclone formation in the Strait of Malacca region.

Although Tropical Cyclone SENYAR remained dynamically immature during the disturbance phase, the combination of persistently warm sea surface temperatures, increasing convective instability, abundant low-level moisture, and weak vertical wind shear established a favorable preconditioning environment for rainfall enhancement. While organized extreme rainfall had not yet fully developed at this stage, these conditions played a crucial role in priming the atmosphere by increasing moisture availability and convective potential. This pre-conditioning set the foundation for the rapid escalation of rainfall intensity observed during the subsequent mature and landfall phases.

3.2.2. Mature Phase

According to the IBTrACS best-track dataset, Tropical Cyclone SENYAR entered its mature phase on 25 November 2025 at 12 UTC. At this time, the system is located near 4.7°N and 99.0°E, with a maximum sustained wind speed of approximately 35 kt and a minimum central pressure of about 999 hPa.

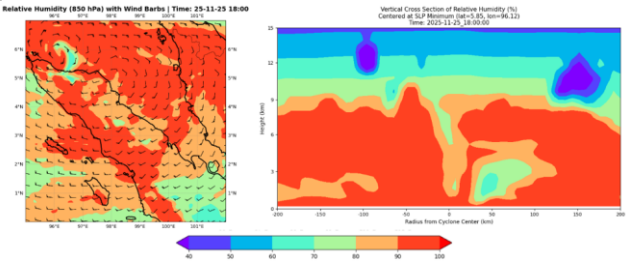

Figure 10. Relative humidity at 850 hPa (left) and vertical cross-section (right) through the cyclone center on 25 November 2025, 18 UTC.

During the mature phase, the evolution of relative vorticity and surface pressure clearly illustrates the favorable conditions for the cyclone's dynamic structure. By 12 UTC on November 25, 2025, WRF simulations indicate that positive relative vorticity **(Figure 9)** had intensified and become more spatially concentrated around the system's center, indicating a strengthening of the low-level cyclonic circulation. When combined with the mean sea level pressure field at this time, the pressure pattern begins to show newly emerging closed isobars with a minimum value around 996 hPa. Further, by 18 UTC on November 25, 2025, this dynamical association becomes much stronger. Relative vorticity remains strongly positive and intensifies near the cyclone's center, while the MSLP field shows a series of well-defined closed isobars with a lower central pressure around 994 hPa. The intensification of the isobaric

pattern reflects an increasing horizontal pressure gradient, which is dynamically consistent with the observed strengthening of the cyclone during this period. The strengthening of the positive relative vorticity and the lowering of the surface pressure indicate that the vortex has become dynamically organized, with efficient low-level convergence and continued heating.

In its mature stage, the relative humidity (RH) **(Figure 10)** clearly reflects a distinct thermodynamic core when viewed from both a spatial and vertical perspective. The horizontal distribution of the RH field, indicated by the lower-layer wind pattern, indicates that very high humidity values, generally exceeding 85–90%, are concentrated around the cyclone's center. These areas of high humidity are accompanied by counterclockwise cyclonic circulation, indicating efficient inward moisture transport toward the core. The interplay of high RH and the wind field indicates active lower-layer moisture convergence, supporting organized deep convection in the inner core region. The WRF simulation of the vertical RH cross-section at 18 UTC also shows a similar pattern. A deep, nearly continuous moisture column extends from the near-surface layer through the middle troposphere and into the upper layers around the cyclone's center. The dry conditions around the cyclone's center also indicate a cyclonic structure consisting of an eye and rainbands. This type of vertically saturated structure is characteristic of mature tropical cyclones and supports the continued release of latent heat, which in turn can strengthen the cyclone's intensity.

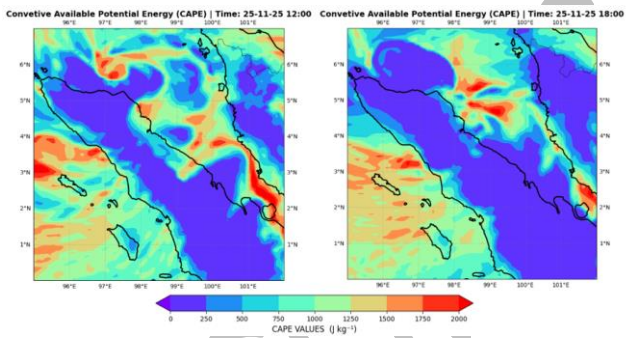

Figure 11. CAPE (J kg^{-1}) on 25 November 2025 at 12 and 18 UTC during the mature phase.

Based on the WRF simulation at 12 UTC on 25 November 2025, CAPE values **(Figure 11)** exceeding 2000 J kg^{-1} are widespread over the marine area surrounding the cyclone core. Such high CAPE indicates a highly unstable atmosphere that is strongly conducive to deep and vigorous convection. This instability supported efficient latent heat release, reinforcing the low-level circulation and intensification. By 18 UTC on 25 November 2025, CAPE values begin to decrease compared to earlier hours, although they remain sufficiently high to sustain convective activity within the cyclone. The reduction in convective instability is spatially consistent with the cyclone's proximity to land, as the system starts to interact with the surrounding landmass and approaches landfall. Surface friction, reduced moisture fluxes from the ocean, and increased boundary-layer heterogeneity associated with land surfaces.

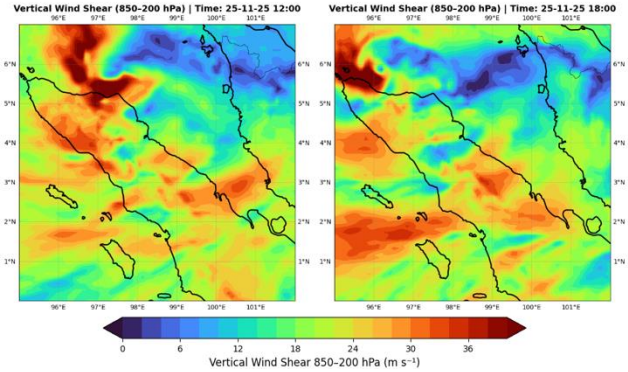

Figure 12. Vertical wind shear (200–850 hPa) on 25 November 2025 at 12 and 18 UTC.

The vertical wind shear pattern **(Figure 12)** during the mature phase of Tropical Cyclone SENYAR further explains the system's ability to maintain its structure as it approached land. WRF results indicate that vertical wind shear remained relatively weak around the cyclone's core, despite higher shear values in the surrounding environment. The low vertical wind shear resistance above the cyclone's center allowed the vortex to remain vertically aligned, preventing tilting and convective disruption that could weaken the system. This configuration supported the maintenance of organized deep convection and sustained cyclonic circulation, allowing Tropical Cyclone SENYAR to remain growing and relatively strong as it moved toward landfall. Overall, the favorable vertical shear environment within the cyclone's core played a key role in allowing the cyclone to persist and maintain its intensity until the point of interaction with land.

The WRF model produced higher maximum wind speeds (50 knots) than the IBTrACS data (35 knots). This difference suggests that the model tends to over-intensify cyclones. This systematic bias can be attributed to the model's high resolution—which can resolve sharp pressure gradients—and the choice of physical parameterization (**Table 1**). The Purdue-Lin and Kain-Fritsch microphysics and convection schemes tend to produce stronger adiabatic heating. However, the YSU boundary layer scheme may underrepresent wind energy dissipation over the ocean. The result is simulations of deeper minimum pressure and stronger surface winds. Spatial cross-section analysis confirms the structure of a mature cyclone, with maximum wind speeds concentrated around the eye in a characteristic ring pattern that indicates dynamically compact and coherent circulation.

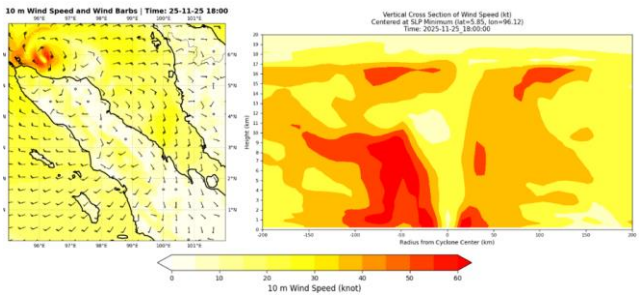

Figure 13. Horizontal wind speed and streamlines at 850 hPa on 18 UTC on 25 November 2025.

A vertical cross-section **(Figure 13)** analysis provides additional insight into the three-dimensional structure of the wind field. WRF simulations indicate that the maximum wind speeds occur approximately 50–100 km from the cyclone's eye, which is consistent with the maximum wind radius (RMW). Together with the deep, vertically aligned wind structure up to an altitude of ~10 km, this pattern confirms a mature feedback mechanism between convection and cyclone dynamics. Strong surface wind convergence, reflected in the pressure gradient in Figure 6, supplies vorticity and moisture. Meanwhile, upward convective momentum transport distributes kinetic energy, maintaining the deep, coherent circulation characteristic of mature tropical cyclones.

The integration of spatial and vertical wind field analysis confirms the maturity of Tropical Cyclone SENYAR's dynamics, reflected in its deep vortex structure and clearly defined maximum wind radius. While the WRF simulation overestimates the maximum wind speed relative to IBTrACS, it successfully captures the key structural characteristics of a mature cyclone, including a compact core, a well-defined radius of maximum wind, and a deep vertically aligned circulation. These results suggest that WRF provides a physically consistent representation of the wind structure during the mature phase, although caution is required when interpreting absolute wind magnitudes.

The mature phase represents the period during which Tropical Cyclone SENYAR exerted its strongest influence on regional rainfall. The vertically aligned vortex, intense low-level convergence, deep moisture columns, and high convective instability collectively facilitated efficient moisture transport and sustained latent heat release. These conditions are physically consistent with the occurrence of widespread and intense rainfall observed over northern Sumatra. Thus, beyond reflecting peak cyclone intensity, the mature phase also marks the critical stage at which extreme rainfall hazards reached their maximum severity.

3.2.3. Landfall Phase

According to IBTrACS data, the landfall phase commenced at 00 UTC on 26 November 2025 and persisted until approximately 12 UTC, marking a critical transition from an ocean-supported system to a land-influenced cyclone. The landfall evolution is characterized by systematic changes in both dynamical and thermodynamical structures, as captured by the WRF simulation. When a cyclone interacts with land, drastic changes occur. Surface pressure at the cyclone's core increases significantly, while low-level vorticity weakens and loses spatial coherence. This marks the beginning of the cyclone's disintegration. Prior to landfall, Tropical Cyclone SENYAR still possessed cyclonic vorticity values supported by strong diabatic heating over warm ocean waters. However, after crossing the coastline, the values of vorticity and air pressure began to weaken in intensity.

The overlay of MSLP and relative vorticity fields **(Figure 14)** indicates that the previously closed isobaric structure becomes progressively less organized, while vorticity maxima weakens and fragment. This evolution reflects the breakdown of the warm-core structure and is consistent with contemporary studies demonstrating that land surface roughening and drying suppress the diabatic feedbacks necessary to sustain cyclonic circulation after landfall.

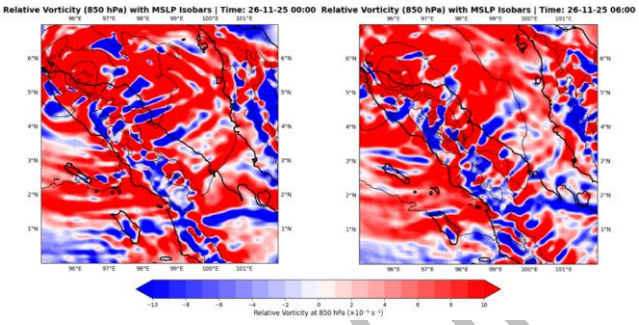

Figure 14. Relative Vorticity with Mean Sea Level Pressure on 26 Nov 2025 at 00 and 06 UTC

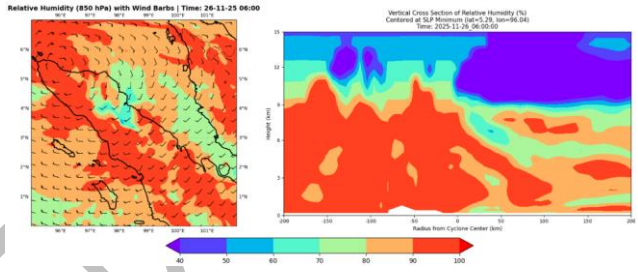

Figure 15. Spatial and cross-section of relative humidity on 26 Nov 2025 at 06 UTC

The landfall phase of Tropical Cyclone SENYAR was accompanied by a marked reduction in atmospheric humidity, particularly in the lower to middle troposphere, as the system transitioned from an oceanic to a continental environment. The spatial distribution of relative humidity at 850 hPa **(Figure 15)**, superimposed on the low-level wind vectors, showed a marked weakening of the moisture inflow towards the cyclone core after SENYAR moved overland. The previously well-organized cyclonic circulation was disrupted by increased surface friction, leading to reduced moisture convergence over the system's center. At the same time, the influx of relatively drier continental air further contributed to the moisture reduction in the surrounding environment.

Analysis of vertical cross sections provides further evidence of this moisture degradation. During landfall, the thick moisture column that characterizes the mature phase, extending from the boundary layer to the upper troposphere, shrinks significantly and becomes vertically discontinuous. Under these conditions, the boundary pattern between the cyclone's eye and the rainband disappears. High relative humidity values are largely confined to the lower troposphere, while humidity in the middle layers decreases substantially. This vertical drying suppresses the development of deep, sustained convection and limits the release of latent heat within the cyclone core.

Consistent with the observed moisture reduction, CAPE values **(Figure 16)** decline significantly during landfall. While the mature phase exhibited large CAPE values

supported by strong surface fluxes over warm seas, the inland environment lacks sufficient heat and moisture to sustain high convective instability. The WRF results show that CAPE decreases rapidly after landfall, indicating a stabilization of the boundary layer and a transition toward shallower, less organized convection. This reduction in convective instability weakens vertical mass fluxes and limits diabatic heating within the cyclone core, further contributing to the collapse of the secondary circulation.

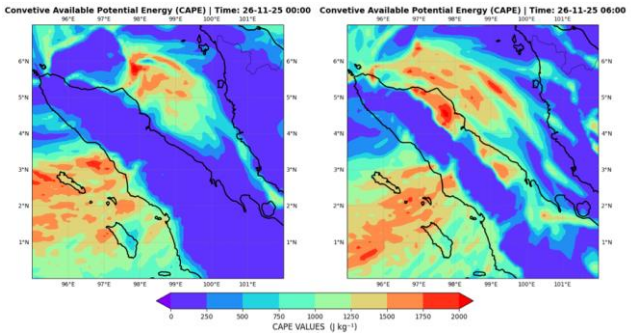

Figure 16. CAPE (J kg^{-1}) on 26 November 2025 at 00 and 06 UTC during landfall.

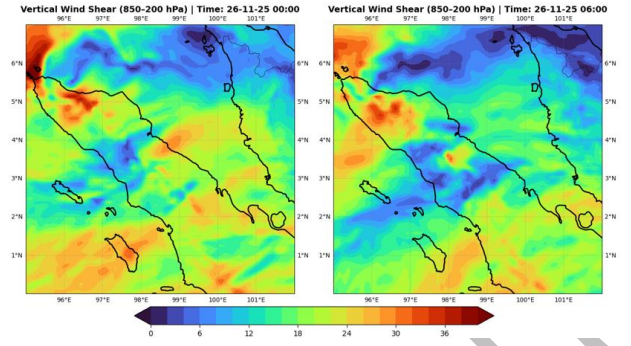

Figure 17. Vertical Wind Shear 850 - 200 hPa on 26 Nov 2025 at 00 and 06 UTC

During the landfall phase, vertical wind shear **(Figure 17)** over and around Tropical Cyclone SENYAR becomes effectively more influential as the system moves inland. Although the large-scale shear does not increase dramatically, WRF results indicate relatively higher shear values over land compared to the cyclone core, which becomes increasingly vulnerable as its circulation weakens. Enhanced surface friction and reduced moisture supply diminish the vertical coherence of the vortex, making it less resistant to shear-induced deformation. As a result, the cyclone experiences increased vortex tilting and convective asymmetry, with deep convection displaced away from the centre. This process disrupts the wind balance and reduces diabatic heating near the core, accelerating the weakening of the warm-core structure. Overall, the increased impact of vertical wind shear during landfall plays a key role in the rapid decay of Tropical Cyclone SENYAR after it moves over land.

Based on the WRF simulations, the landfall phase of Tropical Cyclone SENYAR is characterized by a pronounced weakening of both spatial and vertical wind structures. Spatial wind fields **(Figure 18)** indicate that wind speeds, which were previously strongest within the rainband region during the mature phase, decrease substantially as the cyclone moves over land. The reduction in wind intensity is particularly evident near the former radius of maximum winds, reflecting the rapid dissipation of kinetic energy due to enhanced surface friction and terrain interaction. Vertical cross-section analyses further reveal a collapse of the vertical wind structure during landfall. Prior to land interaction, strong winds extended from the surface to the mid- and upper troposphere, indicating a vertically coherent vortex. However, during landfall, maximum wind speeds become confined to a shallow layer near the surface and diminish rapidly with height.

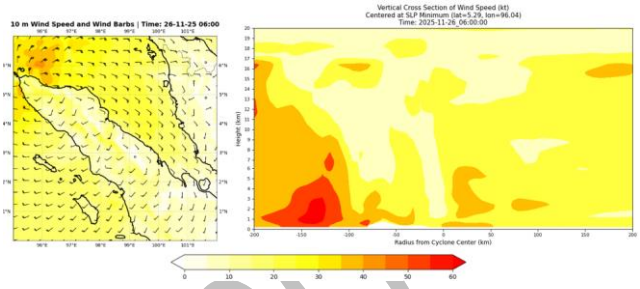

Figure 18. Horizontal wind speed and streamlines at 850 hPa on 26 Nov 2025 at 06 UTC.

3.2.4. Dissipation Phase

The dissipation phase of Tropical Cyclone SENYAR represents the final stage of its life cycle, during which the system loses its coherent tropical cyclone structure and transitions into a weak remnant low. This phase is primarily governed by the combined effects of land interaction, reduced oceanic heat and moisture supply, increasing dynamical imbalance, and progressive thermodynamic stabilization of the atmosphere. Based on IBTrACS data, Tropical Cyclone SENYAR dissipated at 12 UTC on 28 November 2025, marking the end of its identifiable tropical cyclone characteristics. Consistent with this observational record, the WRF simulation captures the dissipation phase as a period of systematic weakening across all key thermodynamic and dynamical indices, as discussed below

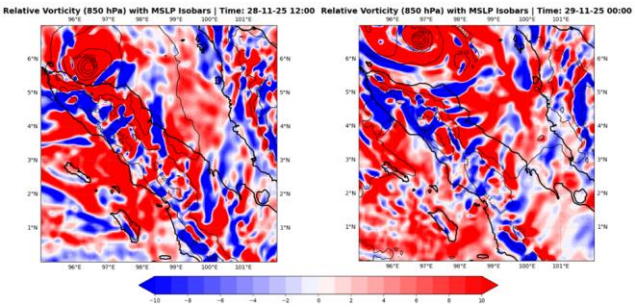

Figure 19. Relative Vorticity + Mean Sea Level Pressure on 28 Nov 2025 at 12 UTC and 29 Nov 2025 at 00 UTC

During the dissipation phase, the WRF results show a continued increase in mean sea level pressure over the former cyclone centre, indicating the collapse of the surface low. Closed isobars that were evident during the mature and early landfall phases become increasingly diffuse and eventually disappear, reflecting the loss of a dynamically consolidated pressure system. When overlaid with relative vorticity **(Figure 19)**, the weakening pressure field is accompanied by a marked reduction in low-level cyclonic vorticity. Positive relative vorticity values diminish in magnitude and become spatially fragmented, indicating

the breakdown of the organized rotational structure. The decoupling between surface pressure and vorticity highlights the transition from a coherent tropical cyclone to a disorganized remnant circulation.

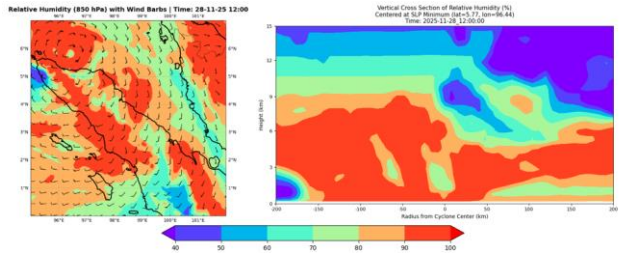

Figure 20. Spatial and Cross-section of Relative Humidity on 28 Nov 2025 at 12 UTC

During the dissipation phase, atmospheric moisture around Tropical Cyclone SENYAR shows contrasting behavior in the horizontal and vertical structures. Spatially, relative humidity at the 850 hPa level **(Figure 20)** remains relatively high over a broad area, indicating that moist air is still present around the remnant circulation. This suggests that, even in the dissipation stage, the near-surface environment retains sufficient moisture, particularly over regions adjacent to the former cyclone track. However, vertical cross-section analyses reveal a different picture. The vertical distribution of relative humidity becomes increasingly shallow, with high RH values largely confined to the lowest atmospheric layers. Moisture in the mid- and upper troposphere decreases noticeably, indicating progressive drying aloft. This thinning of the moist column limits the development of deep convection, reduces latent heat release, and weakens the overall circulation.

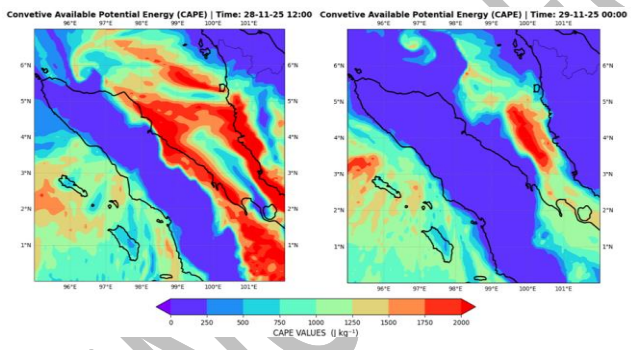

Figure 21. CAPE (J kg^{-1}) on 28–29 November 2025 during dissipation.

Based on the WRF simulation at 12 UTC on 28 November 2025, CAPE **(Figure 21)** in the vicinity of the remnant circulation are very low, indicating a thermodynamically stable atmosphere. Such weak convective instability is insufficient to generate strong or persistent updrafts, thereby limiting the release of latent heat that is essential for maintaining or strengthening the cyclone's circulation. As a result, convective activity becomes shallow and sporadic, preventing any redevelopment of the system.

In the dissipation stage of Tropical Cyclone SENYAR, the role of vertical wind shear becomes increasingly significant in accelerating the weakening of the system. Based on the WRF simulation results on 28 November 2025at 12 UTC and 29 November 2025 at 00 UTC, the vertical wind shear pattern between the 850 hPa and 200 hPa **(Figure 22)** layers shows an increasing destructive influence on the cyclone structure, although the absolute shear values are not always regionally extreme. Spatial analysis shows that the circulation center is experiencing increasing vertical misalignment, with convection being pushed away from the center of minimum pressure. As a result, latent heat release is no longer focused above the cyclone core, rendering the vorticity strengthening mechanism through vorticity stretching ineffective. Furthermore, the increased shear effect relative to the vortex strength leads to vortex tilting, which triggers fragmentation of the convective structure and asymmetry of the system. This condition is reflected in the weakening of the coupling between the lower and upper atmosphere, characterized by reduced upper-level outflow and a weakening of the cyclonic circulation in the middle layers. Thus, although the vertical wind shear value does not increase drastically synoptically, its influence becomes dominant due to the weak dynamic resistance of the system during the dissipation stage.

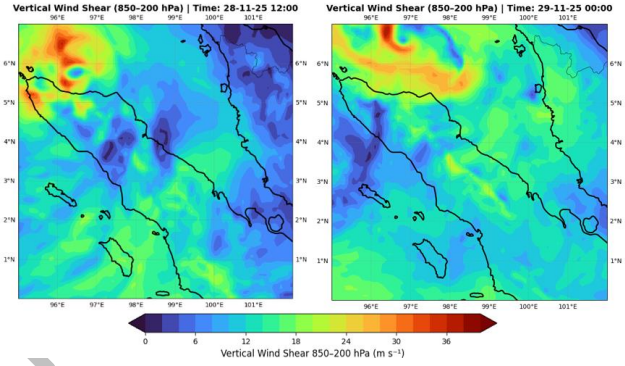

Figure 22. Vertical wind shear on 28–29 November 2025 (dissipation).

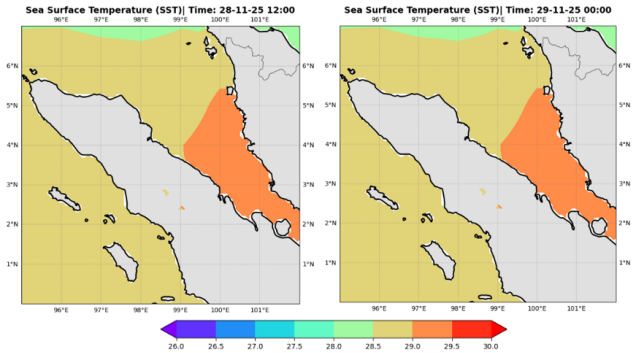

Figure 23. Vertical Wind Shear 850 - 200 hPa on 28 Nov 2025 at 12 and 29 Nov 2025 at 00 UTC

In addition to atmospheric dynamics, Sea Surface Temperature conditions also indirectly contribute to the dissipation stage of Tropical Cyclone SENYAR. Based on WRF simulation results on 28 November 2025 at 12 UTC and 29 November 2025, at 00 UTC **(Figure 23)**, the waters surrounding the remaining system's trajectory showed SST conditions that were no longer warm enough and spatially inhomogeneous to sustain the cyclone's intensification process. During this period, SENYAR had moved away from open waters with high ocean energy content, so it was no longer above a thermodynamically favorable marine environment for system strengthening. During the disspation phase, the system's interaction with land causes

a disconnection of the supply of latent heat and water vapor from the ocean surface. Although climatologically, SST values in the surrounding region remain within the tropical range, WRF simulations at both times indicate that sea surface temperatures are relatively lower and unevenly distributed around the remnant circulation center. This condition indicates a weakening of the latent and sensible heat fluxes from the ocean to the atmosphere. Consequently, the ocean's thermodynamic support for convection and the maintenance of the warm-core structure is severely limited, accelerating Tropical Cyclone SENYAR's weakening and dissipation.

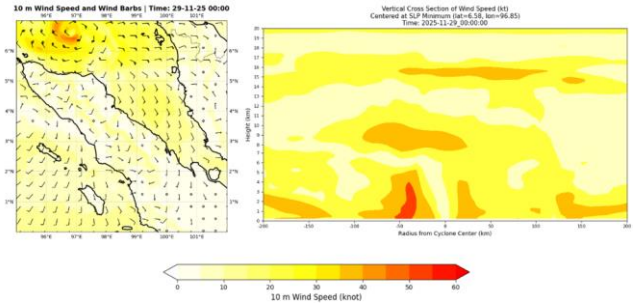

Figure 24. Vertical wind shear 850 - 200 hPa on 29 Nov 2025 at 00 UTC

In response to these increasingly unfavorable environmental conditions, the wind field weakened significantly during the dissipation phase. Wind speeds around the residual circulation decreased substantially, reflecting the loss of dynamic and thermodynamic support for maintaining strong winds. Spatial analysis and vertical cross-sections **(Figure 24)** showed that maximum wind speeds were significantly lower than during the mature and landfall phases, while the remaining circulation structure became increasingly weak and fragmented. This decrease in wind intensity confirmed that atmospheric conditions during the dissipation phase were no longer conducive to maintaining, let alone reintensifying, a tropical cyclone system, thus reinforcing SENYAR's transition to a fully dissipated residual system.

3.3. *Analysis of Extreme Rainfall and Hydrometeorological Impacts*

The extreme rainfall patterns associated with Tropical Cyclone SENYAR can be directly interpreted as the atmospheric response to the dynamical and thermodynamical evolution described in the preceding sections. The intensification of low-level convergence, deep moisture transport, and sustained convective activity during the mature and landfall phases translated into prolonged and spatially extensive rainfall over northern Sumatra. In this section, the rainfall distribution and associated hydrometeorological impacts are analyzed to demonstrate how the evolving cyclone dynamics manifested as severe flooding and landslide hazards in the affected regions.

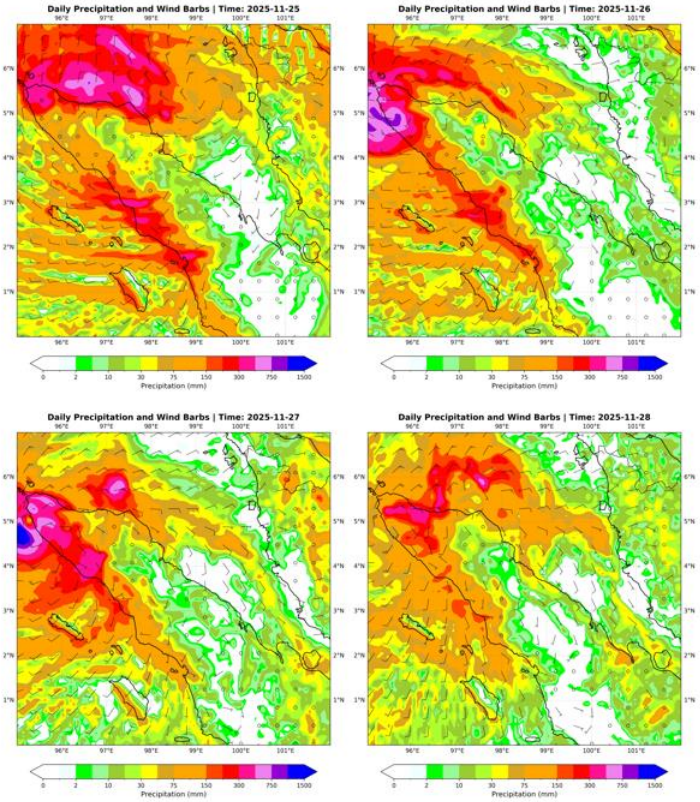

Figure 25. Daily precipitation (mm day^{-1}) and 850-hPa wind barbs from 25 to 28 November 2025.

Figure 25 presents the daily precipitation and wind barbs from 25 to 28 November 2025. The series of daily precipitation maps over 25–28 November 2025 clearly indicate a prolonged and anomalously strong rainfall signal over northern Sumatra, coinciding with the presence and evolution of Tropical Cyclone SENYAR. On 25 November,

precipitation fields reveal an extensive area of moderate to heavy rainfall (>50–100 mm/day) extending across Aceh and North Sumatra, with the most intense values concentrated to the northwest of the Strait of Malacca. These rainfall maxima align with enhanced low-level wind convergence associated with the nascent cyclonic circulation, supporting initial convective development in the pre-genesis and early cyclogenesis stages.

By 26 November, as the system intensified into a tropical cyclone and approached landfall, the spatial precipitation signal strengthens markedly, with widespread rainfall exceeding 150–200 mm/day over Aceh, northern Sumatra, and extending inland toward West Sumatra. The winds depicted in the barbs overlay indicate persistent cyclonic flow providing moisture transport into the region. This pattern correlates strongly with BMKG reports of heavy to extreme rainfall and continuous daily precipitation in Sumatra, where multiple rain gauge stations recorded extreme daily totals on 25-26 November 2025 at Malikussaleh Meteorological Station (310 mm), Maimun Saleh Meteorological Station (162 mm) and Iskandar Muda Meteorological Station (147.3 mm), attributed directly to the influence of Tropical Cyclone SENYAR on regional weather patterns.On 27 November, despite the cyclone moving inland or weakening over land, the precipitation field remains anomalously high. The rainband and convergence zone extend farther inland, maintaining heavy rainfall (>100–150 mm/day) over Aceh and North Sumatra. By 28 November, rainfall intensity began to diminish. The spatial pattern indicates weaker but still widespread rainfall, consistent with the transition of SENYAR into a remnant system with reduced convective intensity. In summary, the daily precipitation and wind barbs from 25 to 28 November clearly illustrate the synoptic-to-mesoscale rainfall forcing associated with Tropical Cyclone SENYAR, including the establishment of persistent rainfall bands and strong moisture convergence. Spatial maxima correlates with areas that subsequently experienced catastrophic flooding and landslides, demonstrating the critical linkage between cyclone-induced precipitation anomalies and observed hydrometeorological impacts in northern Sumatra.

To provide further validation that the extreme rainfall characteristics of SENYAR are physically representative of rare equatorial cyclones, a qualitative comparison was made with Typhoon Vamei (2001)—the only other documented tropical cyclone to form and track within the equatorial Maritime Continent (Chang *et al.*, 2003; Juneng *et al.*, 2007). Despite different genesis mechanisms (Vamei was primarily triggered by a Borneo vortex–cold surge interaction, whereas SENYAR formed under warm SST, high CAPE, and low vertical wind shear), both cyclones exhibited remarkably similar rainfall behavior. In both cases, extreme daily precipitation exceeding 200 mm occurred during the mature-to-landfall transition, not at peak wind intensity, and flooding/landslides were the dominant impacts rather than wind damage. For Vamei, this resulted in catastrophic flooding in Johor, Malaysia; for SENYAR, the same mechanism caused widespread flooding in Aceh and North Sumatra. The ability of WRF-ARW to reproduce these common hydrometeorological characteristics—despite known intensity biases documented in Section 3.5—provides independent, process-based validation that our SENYAR simulation captures the essential dynamics of equatorial cyclogenesis and its rainfall hazards.

4. Conclusion

This study provides the first high-resolution WRF-ARW simulation-based analysis of Tropical Cyclone SENYAR, a rare landfalling cyclone in the Malacca Strait. Three main scientific contributions emerge. First, we quantitatively establish phase-specific thresholds for cyclogenesis in an equatorial maritime environment: CAPE >2000 J kg^{-1} and 850-hPa relative vorticity >10×10^{-5} s^{-1}, under weak vertical wind shear (<10 m s^{-1}). Second, systematic evaluation against IBTrACS reveals that WRF with Purdue-Lin microphysics, Kain-Fritsch cumulus, and YSU boundary layer systematically underestimates minimum sea level pressure by −11.4 hPa (MBE) and overestimates maximum wind speed by +28.04 kt. When compared to existing works, this intensity overestimation aligns with the findings of Shenoy *et al.* (2021), who observed that similar physical parameterization suites tend to over-intensify cyclones due to excessive adiabatic heating in the cyclone core. Third, we demonstrate that extreme rainfall (>200 mm/day) over northern Sumatra is governed by moisture convergence during the mature-to-landfall transition rather than wind intensity alone. This >200 mm/day numerical threshold is highly consistent with the observed hydrometeorological impacts of the only other documented equatorial storm, Typhoon Vamei (2001), validating that our simulation successfully captures the unique dynamics of equatorial cyclones.

Despite these contributions, limitations include the use of a single physics suite, 9-km resolution (insufficient for eyewall processes), and validation based on only three rain gauge stations. To address these limitations, the findings of this study establish a critical operational benchmark for both real-time implementation and the future scope of research. For real-time implementation, identifying the systematic biases of this specific WRF configuration—namely the overestimation of core wind speeds coupled with the accurate representation of extreme rainfall (>200 mm/day) during the mature-to-landfall transition—is highly valuable for operational forecasting. Meteorological agencies can utilize this framework to confidently issue early warnings for hydrometeorological hazards (such as severe flooding and landslides in northern Sumatra) based on the reliable moisture convergence outputs, while applying necessary calibration factors to the wind intensity forecasts. Future works should focus on assimilating regional radar and satellite observations to improve the initial boundary conditions in the data-sparse Malacca Strait, potentially mitigating the observed intensity biases. Furthermore, subsequent research must prioritize coupling these high-resolution WRF rainfall outputs with localized hydrological models (e.g., HEC-HMS, CREST). This coupling will enable the development of real-time, automated flood inundation mapping, effectively bridging process-based

atmospheric modeling with tangible, operational disaster risk reduction strategies in Indonesia.

5. Acknowledgement

The authors would like to thank the reviewers for their constructive comments and suggestions that improved the quality of this manuscript. We also acknowledge the technical support provided by the Department of Physics, Sebelas Maret University, and the Indonesian Agency for Meteorology, Climatology, and Geophysics (BMKG) during the data processing this research.

Dataset Access and Availability

This study utilized three primary datasets included: 1) The NCEP FNL Operational Global Analysis dataset was used as initial and lateral boundary conditions for WRF-ARW simulations, url: https://gdex.ucar.edu/datasets/d083002/dataaccess/. 2) The International Best Track Archieve for Climate Stewardship (IBTrACS) provides global tropical cyclone position and intesity data, URL: https://www.ncei.noaa.gov/products/international-best-track-archive. 3) WRF Model Outputs.

Declaration of generative AI in scientific writing

The authors admit that generative AI tools, such as QuillBot and ChatGPT from OpenAI, were used in the development of this work, particularly for grammar and language editing. AI did not create any content or evaluate any data. The content and conclusions of this work are entirely the authors' responsibility.

References

Auliya, M. N., & Mulya, A. (2021). Hail identification based on weather factor analysis and Himawari 8 satellite imagery (case study of hail on 2nd march 2021 in Malang Indonesia). *International Journal of Remote Sensing and Earth Sciences*, *18*(2), 217-228.

Azgha, R. (2019, June). Analysis of the influence of tropical cyclones on rainfall in Indonesia. In *IOP Conference Series: Earth and Environmental Science* (Vol. 271, No. 1, p. 012035). IOP Publishing.

Biswasharma, R., Umakanth, N., Pongener, I., Longkumer, I., Rao, K. M. M., Pawar, S. D., ... & Sharma, S. (2024). Sensitivity analysis of cumulus and microphysics schemes in the WRF model in simulating Extreme Rainfall Events over the hilly terrain of Nagaland. *Atmospheric Research*, *304*, 107393. https://doi.org/10.1016/j.atmosres.2024.107393.

Bousquet, O., Barruol, G., Cordier, E., Barthe, C., Bielli, S., Calmer, R., ... & Marquestaut, N. (2021). Impact of tropical cyclones on inhabited areas of the SWIO Basin at present and future horizons. part 1: overview and observing component of the research project RENOVRISK-CYCLONE. *Atmosphere*, *12*(5), 544. https://doi.org/10.3390/atmos12050544.

Camargo, S. J., Giulivi, C. F., Sobel, A. H., Wing, A. A., Kim, D., Moon, Y., ... & Zhao, M. (2020). Characteristics of model tropical cyclone climatology and the large-scale environment. *Journal of Climate*, 33(11), 4463-4487. https://doi.org/10.1175/JCLI-D-19-0500.1.

Chang, C. P., Liu, C. H., & Kuo, H. C. (2003). Typhoon Vamei: An equatorial tropical cyclone formation. Geophysical Research Letters, 30(3), 1150.

Chen, S. H., & Sun, W. Y. (2002). A one-dimensional time dependent cloud model. *Journal of the Meteorological Society of Japan. Ser. II*, *80*(1), 99-118. https://doi.org/10.2151/jmsj.80.99.

Dudhia, J. (1989). Numerical study of convection observed during the winter monsoon experiment using a mesoscale two-dimensional model. Journal of Atmospheric Sciences, 46(20), 3077-3107.

Fauzi, R. R., & Hidayat, R. (2018). Role of cold surge and MJO on rainfall enhancement over Indonesia during East Asian winter monsoon. *In IOP Conference Series: Earth and Environmental Science* (Vol. 149, No. 1, p. 012045). IOP Publishing. https://doi.org/10.1088/1755-1315/149/1/012045.

Hanifa, R., & Wiratmo, J. (2024). ENSO and IOD influence on extreme rainfall in Indonesia: historical and future analysis. *Agromet*, 38(2), 78-87. https://doi.org/10.29244/j.agromet.38.2.78-87.

Hong, S. Y., Noh, Y., & Dudhia, J. (2006). A new vertical diffusion package with an explicit treatment of entrainment processes. *Monthly weather review*, *134*(9), 2318-2341. https://doi.org/10.1175/MWR3199.1.

IBTrACS Website. (2025). https://ncics.org/ibtracs/index.php?name=v04r01-2025330N05099 Accessed 22-12-2025.

Ikram, F., Ullah, K., & Chen, D. (2022). Evaluation of Three Genesis Potential Indices for Tropical Cyclogenesis in the Arabian Sea: Two Case Studies Using WRF and ERA5. Monthly Weather Review, 150(12), 3275-3303.

Juneng, L., Tangang, F. T., & Reason, C. J. C. (2007). Numerical case study of an extreme rainfall event. Meteorology and Atmospheric Physics, 98(1), 81–98.

Kain, J. S. (2004). The Kain–Fritsch convective parameterization: an update. *Journal of applied meteorology*, *43*(1), 170-181. https://doi.org/10.1175/1520-0450(2004)043<0170:TKCPAU>2.0.CO;2.

Krisnayanti, D. S., Rozari, P. D., Garu, V., Damayanti, A., Legono, D., & Nurdin, H. (2022). Analysis of flood discharge due to impact of tropical cyclone. *Civil Engineering Journal*, *8*(9), 1752-1763.

Kumar, A., & Singh, R. (2024). Integrated Early Flood Prediction using Sentinel-2 Imagery with VANET-MARL-based Deep Neural RNN. Global NEST Journal, 26(10). https://doi.org/10.30955/gnj.06554.

Lee, J., Im, J., & Shin, Y. (2024). Enhancing tropical cyclone intensity forecasting with explainable deep learning integrating satellite observations and numerical model outputs. *Iscience*, *27*(6). https://doi.org/10.1016/j.isci.2024.109905.

Li, Z., Fung, J. C., Wong, M. F., Lin, S., Cai, F., Lai, W., & Lau, A. K. (2024). Future changes in intense tropical cyclone hazards in the Pearl River Delta region: an air-wave-ocean coupled model study. *Natural Hazards*, *120*(8), 7139-7154. https://doi.org/10.1007/s11069-024-06510-7.

Mlawer, E. J., Taubman, S. J., Brown, P. D., Iacono, M. J., & Clough, S. A. (1997). Radiative transfer for inhomogeneous atmospheres: RRTM, a validated correlated-k model for the longwave. *Journal of Geophysical Research Atmospheres*, 102(14), 16663–16682. https://doi.org/10.1029/97jd00237.

Mulyana, E., Prayoga, M. B. R., Yananto, A., Wirahma, S., Aldrian, E., Harsoyo, B., ... & Sunarya, Y. (2018). Tropical cyclones characteristic in southern Indonesia and the impact on extreme rainfall event. In *MATEC Web of Conferences* (Vol. 229, p. 02007). EDP Sciences.

National Centers for Environmental Prediction, National Weather Service, NOAA, U.S. Department of Commerce. (2000), updated daily. NCEP FNL Operational Model Global Tropospheric Analyses, continuing from July 1999. *NSF National Center for Atmospheric Research.* https://doi.org/10.5065/D6M043C6. Accessed 22-12-2025.

Nugroho, A. D., & Muzaki, N. H. (2022). Study of surface and vertical sea temperatures during the process of tropical cyclone formation in the territory of Indonesia (case study 2019–2021). *IOP Conf. Ser. Earth Environ. Sci*., 989(1), 012006. https://doi.org/10.1088/1755-1315/989/1/012006.

Osuri, K. K., Mohanty, U. C., Routray, A., Mohapatra, M., & Niyogi, D. (2013). Real-time track prediction of tropical cyclones over the North Indian Ocean using the ARW model. *Journal of Applied Meteorology and Climatology*, 52(11), 2476–2492. https://doi.org/10.1175/JAMC-D-12-0313.1.

Permana, D. S. (2021). Impacts of the MJO on Rainfall at Different Seasons in Indonesia. *In IOP Conference Series: Earth and Environmental Science* (Vol. 893, No. 1, p. 012070). IOP Publishing. https://doi.org/10.1088/1755-1315/893/1/012070.

Prasad, S., *et al.* (2024). An Automatic Data-Driven Long-term Rainfall Prediction using Humboldt Squid Optimized Convolutional Residual Attentive Gated Circulation Model in India. Global NEST Journal, 26(10), 06421.

Rahman, S., Sharmin, N., Rahat, A., Rahman, M., & Rahman, M. (2024). Tropical cyclone warning and forecasting system in Bangladesh: challenges, prospects, and future direction to adopt artificial intelligence. *In Computational Urban Science* (Vol. 4, Issue 1). Springer. https://doi.org/10.1007/s43762-023-00113-x.

Rusli, M. H. (2026). Reviewing the 5° Latitude Rule: Cyclone Senyar, Rare Equatorial Cyclogenesis, and Implications for Agricultural Risk Assessment in Southeast Asia. *ACS Agricultural Science & Technology*. https://doi.org/10.1021/acsagscitech.5c01186.

Saufina, E., Trismidianto, Risyanto, Fathrio, I., & Harjupa, W. (2021, September). Impact of cross equatorial northerly surge (CENS) on Jakarta heavy rainfall and its interaction with tropical cyclone (Case study: 18-25 February 2020). In *AIP Conference Proceedings* (Vol. 2366, No. 1, p. 050002). AIP Publishing LLC.

Sekaranom, A. B., Putri, N. H., & Puspaningrani, F. C. (2021). The impacts of Seroja Tropical Cyclone towards extreme weather in East Nusa Tenggara. In *E3S Web of Conferences* (Vol. 325, p. 01020). EDP Sciences.

Sharma, N., *et al.* (2025). A Light weighted Dense and Tree structured simple recurrent unit (LDTSRU) for flood prediction using meteorological variables. Global NEST Journal. https://doi.org/10.30955/gnj.06242.

Shenoy, M., Raju, P. V. S., & Prasad, J. (2021). Optimization of physical schemes in WRF model on cyclone simulations over Bay of Bengal using one-way ANOVA and Tukey's test. Scientific Reports, 11(1), 24412.

Silva, L. F. M. da, Deroubaix, A., Brasseur, G. P., & Gioda, A. (2026). Application of WRF-chem for predicting air quality resulting from the formation of photochemical compounds in a subtropical urban environment. *Urban Climate*, 65. https://doi.org/10.1016/j.uclim.2025.102733.

Singh, V., Tiwari, G., Singh, A., Samanta, R., Srivastava, A. K., Bisht, D. S., Routray, A., Singh, S., Patel, S. S., & Lodh, A. (2025). Tropical Cyclones Across Global Basins: Dynamics, Tracking Algorithms, Forecasting, and Emerging Scientometric Research Trends. *In Meteorological Applications* (Vol. 32, Issue 3). John Wiley and Sons Ltd. https://doi.org/10.1002/met.70067.

Skamarock, W. C., Klemp, J. B., Dudhia, J., Gill, D. O., Liu, Z., Berner, J., Wang, W., Powers, J. G., Duda, M. G., Barker, D. M., & Huang, X.-Y. (2019). A Description of the Advanced Research WRF Model Version 4. http://library.ucar.edu/research/publish-technote.

Spiridonov, V., Baez, J., Telenta, B., & Jakimovski, B. (2020). Prediction of extreme convective rainfall intensities using a free-running 3-D sub-km-scale cloud model initialized from WRF km-scale NWP forecasts. *Journal of Atmospheric and Solar-Terrestrial Physics*, *209*, 105401. https://doi.org/10.1016/j.jastp.2020.105401.

Subramanian, S., Rani, G. K., Madhavan, M., & Rajendran, S. (2024). An automatic data-driven long-term rainfall prediction using Humboldt squid optimized convolutional residual attentive gated circulation model in India. Global NEST Journal, 26(10), 06421. https://doi.org/10.30955/gnj.06421

Tridaiana, S., & Marzuki, M. (2023). Exploring the complex dynamics of tropical cyclone activity in the southern indian ocean: a multidecade analysis. *Jurnal Penelitian Pendidikan IPA*, *9*(11), 1069-1077.

Venkatraman, M., Surendran, R., Srinivasulu, S., & Vijayakumar, K. (2024). Water quality prediction and classification using attention based deep differential recurflownet with logistic giant armadillo optimization. Global NEST Journal. https://doi.org/10.30955/gnj.06799.